



Surface assisted laser desorption ionization (SALDI) mass spectrometry
by Yu-Chie Chen

A thesis submitted in partial fulfillment of the requirements for the degree of Doctor of Philosophy in
Chemistry

Montana State University

© Copyright by Yu-Chie Chen (1997)

Abstract:

A new laser desorption ionization technique named "Surface Assisted Laser Desorption Ionization (SALDI) Mass Spectrometry" has been developed. SALDI avoids some drawbacks of the accepted laser desorption ionization method, Matrix Assisted Laser Desorption Ionization (MALDI). Instead of using a solid matrix, a suspension is used in SALDI that is composed of glycerol (SALDI solvent) with a graphite or activated carbon powder (SALDI solid). Sucrose is added to the SALDI suspension as an "adhesive" to immobilize the SALDI solid powder and limit contamination of the ion source.

The mass resolution of SALDI is almost identical with that of MALDI. Furthermore, the detection limit of SALDI is less than 10 fmole for analytes like peptides. However, the mass range is less than 20,000 Da. A very important advantage of SALDI is a low matrix background at low mass range.

Applications of SALDI to the analysis of amino acids, peptides, small proteins, organics, volatile organics, and polymers have been demonstrated. In particular, SALDI is very useful for peptide mixtures such as enzymatic digest products.

Activated carbon is the most useful SALDI solid. Activated carbon is also one of the most common adsorbents used in solid phase-extraction (SPE). The combination of SPE with SALDI has been developed. SPE/SALDI is a fast screening method and can be used for either qualitative or quantitative analysis. Furthermore, the development of TLC/SALDI is explored in this thesis.

SURFACE ASSISTED LASER DESORPTION IONIZATION

(SALDI) MASS SPECTROMETRY

by

Yu-Chie Chen

A thesis submitted in partial fulfillment
of the requirements for the degree

of

Doctor of Philosophy

in

Chemistry

MONTANA STATE UNIVERSITY
Bozeman, Montana

January 1997

D378
C4199

APPROVAL

of a thesis submitted by

Yu-Chie Chen

This thesis has been read by each member of the thesis committee and has been found to be satisfactory regarding content, English usage, format, citations, bibliographic style and consistency, and is ready for submission to the College of Graduate Studies.

Jan Sunner

Jan Sunner
(Signature)

Jan. 16, 1997
Date

Approved for the Department of Chemistry

David M. Dooley

David M. Dooley
(Signature)

1/16/97
Date

Approved for the College of Graduate Studies

Robert L. Brown

RL Brown
(Signature)

2/3/97
Date

STATEMENT OF PERMISSION TO USE

In presenting this thesis in partial fulfillment of the requirements for a doctoral degree at Montana State University-Bozeman, I agree that the Library shall make it available to borrowers under rules of the Library. I further agree that copying of this thesis is allowable only for scholarly purpose, consistent with "fair use" as prescribed in the U.S. Copyright Law. Requests for extensive copying or reproduction of this thesis should be referred to University Microfilms International, 300 North Zeeb Road, Ann Arbor, Michigan 48106, to whom I have granted "the exclusive right to reproduce and distribute my dissertation in and from microform along with the non-exclusive right to reproduce and distribute my abstract in any format in whole or in part."

Signature Yu-Chie Chen

Date 1/16/97

ACKNOWLEDGMENTS

Primary acknowledgment and thanks must go to Dr. Jan Sunner for his patience and help during my years as his student. Thanks are due to Dr. Joe Sears for his great help in maintaining the instrument and invaluable help during my graduate studies. Special thanks are due to Dr. Jentaie Shiea for his invaluable opinions in my research during his sabbatical in Montana State University.

Thanks go to all my committees, Dr. Joe Sears, Dr. Edward Dratz, Dr. K.D. Hapner, Dr. Patrik Callis and Dr. Warren P. Scarrah for their invaluable suggestions in my thesis.

Acknowledgment and thanks go to Kim Tom, Praveena Devi, David Barnidge, Dan Amundson, and Qiang Wu for their friendship and help during these years.

More than thanks are due to my parents, my sister, and my brother. Their support and confidence have helped me immeasurable amount. Without their full support in every aspect, I could have never done it.

The work in this thesis would not have been possible without the help of many people, and it is impossible to thank them all individually here.

TABLE OF CONTENTS

	Page
1. INTRODUCTION	1
General	1
History of Laser Desorption Mass Spectrometry	3
Matrix Assisted Laser Desorption Ionization (MALDI) Mass Spectrometry	4
Advantages of MALDI.	5
Matrices in MALDI	5
Development of Liquid Matrices for Laser Desorption	8
Mechanisms of MALDI	9
Phase Explosion Model	9
Cool Plume Model	10
Homogeneous Bottleneck Model	11
Shock Wave Model	12
Photoionization Model	13
Instrumentation for Laser Desorption (LD) Time of Flight	
Mass Spectrometry	14
Laser Ion Source	14
Time-of-Flight Mass Spectrometry	14
Basic Principles	15
Advantages of TOF/MS.	17
Factors Affecting Mass Resolution of TOF	17
Methods for Improving Mass Resolution in TOF/MS	18
Ion Detectors in TOF/MS	22

TABLE OF CONTENTS – Continued

	Page
Signal Processing	22
Objectives of the Thesis	25
Development of a New Laser Desorption Ionization Method	25
SALDI Solids	25
SALDI Solvents	26
SALDI “Adhesive”	27
SALDI Solvent Effects	27
Applications of SALDI	28
Solid Phase Extraction (SPE)/SALDI	28
Thin Layer Chromatography (TLC)/SALDI	28
2. EXPERIMENTAL	29
Instrumentation	29
Materials	29
Sample Preparation of SALDI	31
3. DEVELOPMENT OF SALDI METHOD	34
Introduction	34
Early SALDI Results	36
SALDI Solids	46
SALDI Solvents	61
SALDI “Adhesive”	69
SALDI Analyte Solvents	76
Internal Energy of SALDI Ions	78
Combining SALDI with MALDI Matrix	81
Optimum SALDI Sample Preparation Conditions	82

TABLE OF CONTENTS – Continued

	Page
Optimum Proportions of SALDI Suspension Compounds	82
Detection Limit of SALDI	91
Mass Range of SALDI	92
4. SALDI SOLVENT EFFECTS	94
Gas Phase Basicity Effects in SALDI	94
Salt Effects in SALDI	102
Acid Effects in SALDI	103
5. APPLICATIONS OF SALDI	110
Analysis of Biochemicals	110
Experimental	111
Results and Discussion	112
Analysis of Polymers and Porphyrins	121
Analysis of Volatile Organic Compounds	126
6. SPE (SOLID PHASE EXTRACTION)/SALDI	134
General	134
SPE/SALDI	135
Sample Preparation of SPE/SALDI	136
Method	136
Summary of SPE/SALDI Procedures	138
Results and Discussion.	139
Qualitative Analysis	139
Analysis of Diuretics	139
Analysis of Herbicides	143
Analysis of Amino Acids and Peptides	145

TABLE OF CONTENTS-Continued

	Page
Quantitative Analysis	149
SPME (Solid Phase MicroExtraction)/SALDI	152
General	152
Sample Preparation of SPME/SALDI	152
Results and Discussion	153
7. THIN LAYER CHROMATOGRAPHY (TLC)/MS	157
Introduction	157
TLC/EI (or CI) MS	159
TLC/PDMS	159
TLC/LSIMS or FAB	160
TLC/LD	161
TLC/MALDI	161
TLC/SALDI	163
Experimental	163
Results and Discussion	165
8. CONCLUSIONS	187
Summaries of Results and Conclusions	187
Development of SALDI	187
SALDI Solvent Effects	188
Applications of SALDI	189
SPE/SALDI	190
TLC/SALDI	191
Future Prospects of SALDI	191
LITERATURE CITED	193

LIST OF TABLES

Table	Page
1. Summary of common matrices in MALDI	7
2. SALDI solid materials	60
3. SALDI solvents	68
4. The abundance ratio of 136/268 in linear TOF mode with different SALDI solids	81
5. Tryptic peptides of cytochrome C	118
6. Absolute detection limits of diuretics in a 3 mL volume of water in the analysis of SPE/SALDI	143
7. Absolute SPE/SALDI detection limits for triazines in pure water solution	143

LIST OF FIGURES

Figure	Page
1. Linear time-of-flight mass spectrometer	16
2. Two stage Mamyrin reflectron (top) and coaxial reflectron (bottom)	21
3. Block diagram of a transient recorder	24
4. Extinction coefficient of graphite as a function of the photon energy in the ultraviolet visible wavelength range.	35
5. Graphite/SALDI (337 nm) mass spectrum of glycerol.	38
6. Graphite/SALDI (337 nm) mass spectrum of a solution of 0.25% (v/v) DEA in Gl.	39
7. Graphite/SALDI mass spectrum (337 nm) of 0.25% DEA in Gl at an elevated laser power setting. The spectrum is dominated by carbon cluster.	41
8. Graphite/SALDI mass spectrum of bradykinin (mw= 1,060.5). Internal mass calibration using Cs ⁺ and Cs ⁺ (bradykinin). Inset shows the bradykinin pseudo-molecular ion region on an expanded scale	43
9. Graphite/SALDI mass spectrum of bradykinin (mw= 1,060.5). Graphite powder was heated on a heating plate for 15 minutes before it was used as the SALDI solid.	44

LIST OF FIGURES-Continued

Figure	Page
10. Graphite/SALDI mass spectrum of cytochrome C (mw= 12,360). Internal mass calibration using Cs ⁺ and Cs ⁺ (cytochrome C)	45
11. Graphite flakes/SALDI mass spectrum of bradykinin (mw= 1,060.5)	48
12. Scanning Electron Microscope (SEM) pictures of the surface of activated carbon (top) and graphite (bottom)	50
13. Activated carbon/SALDI mass spectrum of bradykinin (mw= 1,060.5). The activated carbon granule was ground to a fine powder before being used in the SALDI analysis. The activated carbon was of the gas phase absorption type	52
14. Carbo-pack/SALDI mass spectrum of methionine enkephalin (mw=573.7).	52
15. Fluorinated graphite/SALDI mass spectrum of angiotensin II (mw= 1,046.2)	55
16. Activated carbon/SALDI mass spectrum of bradykinin (mw=1,060.5). A single granule (4-12 mesh) was used	56
17. Activated carbon SALDI mass spectrum of bradykinin (mw= 1,060.5). The granule (4-12 mesh) was ground to a fine powder before being used in the SALDI analysis)	56
18. Activated carbon/SALDI mass spectrum of cytochrome C (mw= 12,360). The granule (4-12 mesh) was ground to powder before using as the SALDI solid.	58

LIST OF FIGURES-Continued

Figure	Page
19. SALDI mass spectrum of angiotensin II (mw= 1,046.2). The SALDI solid was made by vapor deposition of a thin layer of carbon on a PVDF membrane. Analyte solution and SALDI solvent (50% GI/MeOH) were added to the coated membrane	59
20. Activated carbon/SALDI mass spectrum of bradykinin (mw= 1,060.5) without adding any SALDI solvent	62
21. Activated carbon/SALDI mass spectra of angiotensin II (mw=1,046.2) by using NBA, DEA, TEA, GI, thioglycerol, and magic bullet, and PEG 400 as the SALDI solvent	63
22. SALDI mass spectra of cytochrome C (mw= 12,360) by using NBA, DEA, TEA, GI, thioglycerol, magic bullet, and 18-crown-6-ether as the SALDI solvent	66
23. Activated carbon/SALDI mass spectra of angiotensin II (mw= 1,046.2). The SALDI solvents were 4.0 g/mL sucrose/water, 2.0 g/mL sucrose/water, and 1.0 g/mL sucrose/water	72
24. Activated carbon/SALDI mass spectra of angiotensin II (mw=1,046.2) without adding sucrose (top) and with adding 1 μ L of 5% sucrose/water to the SALDI suspension (bottom).	74
25. Activated carbon/SALDI mass spectra of cytochrome C (mw= 12,360), without adding sucrose (top), and with adding 1 μ L of 5% sucrose/water (bottom)	75

LIST OF FIGURES-Continued

Figure	Page
26. Activated carbon/SALDI mass spectra of angiotensin II (mw= 1,046.2) (top) and cytochrome C (mw= 12,360) (bottom) with mannose used to immobilize the SALDI solid	77
27. Activated carbon/SALDI-PSD mass spectrum of adenosine (mw=267.2, 200 nmole) (bottom). MALDI-PSD mass spectrum of adenosine (200 nmole) (top)	79
28. SALDI-MALDI combination mass spectrum of bradykinin (mw= 1,060.5).	83
29. Mass spectrum of bradykinin (mw= 1,060.5) with saturated α -cyano-4-hydroxy cinnamic acid and glycerol (1/1, v/v) as the matrix	84
30. Activated carbon/SALDI mass spectra of bradykinin (mw= 1,060.5) using different concentration glycerol to prepare the SALDI suspension: 15% glycerol/methanol, 30% glycerol/MeOH , and 60% glycerol/MeOH from top to bottom. The ratios of glycerol to activated carbon (w/w) are 75%, 150%, 300%, respectively	86
31. Activated carbon/SALDI mass spectra of bradykinin (mw= 1,060.5) using different concentrations of sucrose in water to immobilize activated carbon powder: 5% sucrose/water, 25% sucrose/water, and 50% sucrose/water from top to bottom	89
32. The same sample as for Figure 24. However, the mass spectra were recorded after the sample had been left in the ion source for 30 minutes	90
33. Activated carbon/SALDI mass spectrum of myoglobin (mw= 16,951)	93

LIST OF FIGURES-Continued

Figure	Page
34. Semilog plot of the intensity of asparagine pseudo-molecular ions in the SALDI mass spectra versus DEA/GI concentration in the SALDI matrix	96
35. Negative ion activated carbon/SALDI mass spectrum of asparagine (mw= 132.1, 0.1 nmol).	97
36. Activated carbon/SALDI mass spectra of cytochrome C (mw= 12,360). The SALDI solvents are GI, DEA, and TEA	98
37. Activated carbon/SALDI mass spectra of cytochrome C (mw= 12,360). Spectra were obtained in the few minutes (top) and after 40 minutes (bottom) of irradiating the same spot with the laser	100
38. Activated carbon/SALDI mass spectrum of angiotensin II (mw= 1,046.2) using DEA as the SALDI solvent	101
39. Activated carbon/SALDI mass spectra of bradykinin (mw= 1,060.5) with varying concentrations of SDS in the SALDI suspension: 0% SDS, 2.5% SDS, and 5.0% SDS from top to bottom	104
40. Activated carbon/SALDI mass spectra of bradykinin (mw= 1,060.5) with varying concentrations of NaCl in the SALDI suspension: 0% NaCl (top) and 1.25% NaCl (bottom)	105
41. Activated carbon/SALDI mass spectra of bradykinin (mw= 1,060.5) with varying concentrations of acetic acid in the SALDI suspension: 0% acetic acid, 0.3% acetic acid, 2.5% acetic acid from top to bottom	107

LIST OF FIGURES-Continued

Figure	Page
42. Activated carbon/SALDI mass spectra of angiotensin II (mw= 1,046.2) with varying concentrations of acetic acid in the SALDI suspension: 0% acetic acid, 0.3% acetic acid, and 2.5% acetic acid from top to bottom	108
43. Graphite/SALDI mass spectrum of peptide mixture. The mixture includes methionine enkephalin (mw= 573.7, 0.1 nmole), bradykinin (mw= 1,060.5, 0.1 nmole), and mellitin (mw= 2,846.5, 0.1 nmole)	113
44. SALDI mass spectrum of methionine enkephalin (mw= 573.7, 0.1 nmole)	114
45. MALDI mass spectrum of a peptide mixture. The mixture includes methionine enkephalin (mw= 573.7, 0.1 nmole), bradykinin (mw= 1,060.5, 0.1 nmole), and mellitin (mw= 2,846.5, 0.1 nmole)	115
46. Activated carbon/SALDI mass spectrum of a peptide mixture. The mixture includes methionine enkephalin (mw= 574, 0.1 nmole), bradykinin (mw= 1,060.5, 0.1 nmole), and mellitin (mw= 2,846.5, 0.1 nmole)	115
47. Graphite/SALDI mass spectrum of tryptic digest of cytochrome C. 0.01% SDS/H ₂ O was added to the SALDI suspension	117
48. Peptide bond hydrolysis by carboxypeptidase	119
49. Activated carbon/SALDI mass spectrum of carboxypeptidase Y digest of bradykinin. The digest reacted for 10 minutes	120
50. Activated carbon/SALDI mass spectrum of carboxypeptidase Y digest of bradykinin. The digest reacted for 110 minutes. Fractions were collected every 10 minutes. The spectrum was obtained from the combination	

LIST OF FIGURES-Continued

Figure	Page
of the 12 product fractions	120
51. Activated carbon/SALDI mass spectrum of polyalanine (mw= 1,000-5,000, 0.01 mg)	122
52. Activated carbon/SALDI mass spectrum of PEGs: PEG 200, PEG 400, PEG 1500, PPG 3000, PEG 4600	123
53. Activated carbon/SALDI mass spectrum of polystyrene (mw _{ave} =2,727). 0.5 M silver nitrate in the SALDI suspension (top). Activated carbon/SALDI mass spectrum of polystyrene (mw _{ave} = 2,727). 0.5 M copper sulfate in the SALDI suspension (middle). Activated carbon/SALDI mass spectrum of polystyrene (mw= 2727). 0.5 M silver nitrate and copper sulfate in the SALDI suspension (bottom)	125
54. Activated carbon/SALDI mass spectrum of 5, 10, 15, 20-tetrakis (pentafluorophe-21H, 23H-porphine iron (III) chloride (mw= 1,063.85)	127
55. Activated carbon/SALDI mass spectrum of 5, 10, 15, 20-tetraphenyl-21H 23H-porphine cobalt (II) (mw= 671.67)	127
56. Activated carbon/SALDI mass spectrum of azulene (100 nmole, mw= 128.16) .	129
57. MALDI mass spectrum of azulene (100 nmole, mw= 128.16)	129
58. LD mass spectrum of azulene (100 nmole, mw= 128.16)	129
59. Activated carbon/SALDI mass spectrum of naphthalene/chloroform (mw= 128.16, 1000 nmole)	130

LIST OF FIGURES-Continued

Figure	Page
60. LD mass spectrum of naphthalene/chloroform (mw= 128.16, 1000 nmole)	130
61. Activated carbon/SALDI mass spectrum of pyridine (mw= 79.09)	132
62. The intensity of azulene molecular ions versus the concentration of azulene based on the SALDI mass spectra	133
63. SPE extractor for small volume extraction solution	137
64. SPE/SALDI mass spectra (negative ion mode) of hydroflumethiazide (mw= 331.29, 3 μ g), dichlorophenamide (mw= 305.16, 30 μ g), furosemide (mw= 330.7, 30 μ g), bumetanide (mw= 364.42, 20 μ g), hydrochlorothiazide (mw= 297.72, 20 μ g). Analyte was added to 3 mL of pure water for each spectrum	140
65. SPE/SALDI mass spectrum (negative ion mode) of diuretics spiked into pure water. The diuretics were hydroflumethiazide (mw= 331.29), hydrochlorothiazide (mw= 297.72), bumetanide (mw= 364.42), and dichlorophenamide (mw= 305.16) 100 μ g of each diuretic was added to 6 mL pure water	142
66. SPE/SALDI mass spectrum of prometryn (mw= 241.37, 50 μ g), atrazine (mw= 215.68, 30 μ g), ametryn (mw= 227.35, 3 μ g), prometon (mw= 225.29, 3 μ g). Each analyte was added to 3 mL of pure water	144
67. SPE/SALDI mass spectrum of prometryn (mw= 241.37). 1000 μ g of prometryn was spiked into 300 mL of pure water	146
68. SPE/SALDI mass spectrum of the river water sample	147

LIST OF FIGURES-Continued

Figure	Page
69. SPE/SALDI mass spectrum of triazines spiked into river water. The triazines include prometryn (mw= 241.37), atrazine (mw= 215.68), ametryn (mw= 227.35), prometon (mw= 225.29). One hundred micro grams of each triazine were added to 3 mL river water	147
70. SPE/SALDI mass spectrum (negative ion mode) of phenylalanine. 100 μ g of phenylalanine was spiked into 3 mL of pure water	148
71. SPE/SALDI mass spectrum of isoleucine (mw= 132.08). One mL of isoleucine solution (0.052 mg/mL) was extracted by SPE	148
72. SPE/SALDI mass spectrum (negative ion mode) of angiotensin II (mw= 1,046.2). Angiotensin II (10 nmole) aqueous solution was extracted by SPE	150
73. The intensity of hydroflumethiazide molecular ions versus the concentration of hydroflumethiazide in SPE/SALDI results	151
74. SPME/SALDI mass spectrum (negative ion mode) of hydrochlorothiazide (mw= 297.72, 50 μ g analyte in 0.5 mL solution)	154
75. SPME/SALDI mass spectrum of hydroflumethiazide (mw= 331.29, 1 μ g analyte in 0.6 mL solution)	154
76. The intensity of dichlorothiazide versus the extraction time in SPME. The intensity of dichlorothiazide molecular ions was detected by the SALDI	156
77. SALDI mass spectrum of SALDI suspension on TLC plate	166

LIST OF FIGURES-Continued

Figure	Page
78. SALDI mass spectrum of bradykinin (1 nmole, mw= 1,060.5) on TLC plate. The analyte was extracted from silica gel. SALDI suspension "A" was added . .	168
79. TLC/SALDI mass spectrum of bradykinin (1 nmole, mw= 1,060.5. The analyte was eluted onto the TLC surface by 70% EtOH/H ₂ O. SALDI suspension "A" was subsequently added	168
80. TLC/SALDI mass spectra of angiotensin II (0.5 nmole). Angiotensin II was extracted from the silica gel by adding 0.5 μ L of glycerol and subsequently adding 0.5 μ L of SALDI suspension A (Top spectrum). A one microliter of glycerol and 0.5 μ L of SALDI suspension B were added to the sample spot (Bottom spectrum)	170
81. SALDI mass spectra of bradykinin (2.5 nmole, mw= 1,060.5) (top) and SALDI mass spectrum of angiotensin II (0.5 nmole, mw= 1,046.2) (bottom). SALDI suspension C (0.5 μ L) was applied to the sample spot, and then 0.5 μ L of glycerol was added	172
82. SALDI mass spectra of angiotensin II (0.5 nmole, mw= 1,046.2) on TLC plate by mixing different ratios of "1" and "2" solution. "1" solution was made by 25 mg of activated carbon powder mixing with 50% glycerol/methanol. "2" solution was made by 5% sucrose/water	173
83. SALDI mass spectra of angiotensin II (0.5 nmole, mw= 1,046.2) on TLC plate without ninhydrin (top) and with ninhydrin (bottom)	175
84. SALDI mass spectrum of angiotensin II (0.5 nmole, mw= 1,046.2) on TLC plate. Dithiothreitol was the extraction solvent	176

LIST OF FIGURES-Continued

Figure	Page
85. SALDI mass spectrum of angiotensin II (0.5 nmole, mw= 1,046.2) on silica gel plastic-backed TLC plate. Threitol was the extraction solution	176
86. The intensity changes of bradykinin protonated molecule in TLC/SALDI versus the different concentrations of sucrose as the extraction solvent	178
87. SALDI mass spectrum of angiotensin II (0.5 nmole, mw= 1,046.2) on silica gel plastic-backed TLC plate. Thioglycerol was the extraction solution	180
88. SALDI mass spectrum of arginine (100 nmole, mw= 174.1) on silica gel plastic-backed TLC plate. Glycerol was the extraction solution	181
89. SALDI mass spectrum of hydrochlorothiazide (1 μ g, mw= 297.72) on TLC plate (negative ion mode)	183
90. SALDI mass spectra of bradykinin (1 nmole, mw= 1,060.5) and hydrochlorothiazide (10 μ g, mw= 297.72) on TLC plate scratched from the TLC plate and mixed with SALDI suspension	184
91. SALDI mass spectra of bradykinin (0.5 ng, mw= 1,060.5) and hydroflumethiazide on silica gel plastic-backed plate. Activated carbon was added by drawing a line with a pencil over the sample spot	185

ABSTRACT

A new laser desorption ionization technique named "Surface Assisted Laser Desorption Ionization (SALDI) Mass Spectrometry" has been developed. SALDI avoids some drawbacks of the accepted laser desorption ionization method, Matrix Assisted Laser Desorption Ionization (MALDI). Instead of using a solid matrix, a suspension is used in SALDI that is composed of glycerol (SALDI solvent) with a graphite or activated carbon powder (SALDI solid). Sucrose is added to the SALDI suspension as an "adhesive" to immobilize the SALDI solid powder and limit contamination of the ion source.

The mass resolution of SALDI is almost identical with that of MALDI. Furthermore, the detection limit of SALDI is less than 10 fmole for analytes like peptides. However, the mass range is less than 20,000 Da. A very important advantage of SALDI is a low matrix background at low mass range.

Applications of SALDI to the analysis of amino acids, peptides, small proteins, organics, volatile organics, and polymers have been demonstrated. In particular, SALDI is very useful for peptide mixtures such as enzymatic digest products.

Activated carbon is the most useful SALDI solid. Activated carbon is also one of the most common adsorbents used in solid phase-extraction (SPE). The combination of SPE with SALDI has been developed. SPE/SALDI is a fast screening method and can be used for either qualitative or quantitative analysis. Furthermore, the development of TLC/SALDI is explored in this thesis.

CHAPTER 1

INTRODUCTION

General

Extension of the mass range to include large molecules has long been an important problem in mass spectrometry. However, larger molecules tend to be polar, nonvolatile, and thermally labile. Traditional ionization methods in mass spectrometry, such as electron impact ionization (EI) and chemical ionization (CI), require high volatility of samples because molecules are ionized in the gas phase. If analytes have a low volatility, their mass and structure cannot be obtained using these traditional ionization methods. Therefore, extensive efforts have been made over many years to invent and develop new ionization methods for low volatility and thermally labile compounds. An ideal soft desorption ionization technique must have the advantages of high sensitivity, low ion background, easy operation, high mass range, etc. The methods that have been developed for this purpose can be divided into spray ionization and desorption ionization (DI) methods. The term "desorption ionization" refers to methods where analyte molecules are desorbed and ionized in a single step in vacuum. Here, we will be concerned solely with DI methods. In all these methods, energy is quickly deposited onto a liquid or solid surface. Ions ejected from the surface are detected by a mass spectrometer.

Several main types of desorption ionization methods have been developed: three types of particle-induced desorption methods and two types of laser-induced desorption methods. Particle-induced desorption methods include Plasma Desorption (PD) (Torgerson et al, 1974; Sundqvist & MacFarlane, 1984), Static Secondary Ion Mass Spectrometry (SIMS) (Benninghoven et al., 1970; Grade & Cooks, 1978), and Fast Atom Bombardment (FAB) (Barber et al., 1981). Each method has its unique advantages and disadvantages. For example, PD has low sensitivity and produces noisy spectra and thus is not used very often anymore. In SIMS, a very high energy ion beam bombards the sample. It is a "harder" desorption ionization method than the other DI methods. SIMS cannot be connected with chromatography in a simple way because solid samples are used. FAB has been interfaced with chromatography, FAB is noisy and has a low mass limit problem. The upper mass limit for all particle-induced DI methods is a few thousand Daltons. Thus, these methods cannot be used to analyze larger biomolecules, such as proteins.

In direct Laser Desorption (LD) (Honing et al., 1963), a pulsed laser is used to desorb analyte molecules and ions from a surface to vacuum. The upper mass range of LD is under 2,000 Da (Linder et al., 1985). This is not sufficient for large biomolecules, such as proteins. Two more recent techniques are ElectroSpray Ionization (ESI) and Matrix Assisted Laser Desorption Ionization (MALDI). Both are softer than the particle induced or the direct laser desorption techniques. In MALDI, a light absorbing material, called matrix, is mixed with the analyte in solution. Upon solvent evaporation, the matrix and analyte co-crystallize. During laser pulse irradiation in a vacuum, a desorption ionization process occurs. In this process, gas phase ions of both matrix and analyte are formed. High molecular weight

molecules, such as proteins, can be analyzed by MALDI or ESI. The maximum mass range in MALDI has been extended above 500 kDa. Partly for these reasons, MALDI and ESI have become revolutionary and practical techniques for routine biochemical structure determinations. Here, the history and mechanisms of LD and MALDI will be described first. Subsequently, the instrumentation will be discussed.

History of Laser Desorption Mass Spectrometry

It was demonstrated already in 1960's that when a laser beam hits a solid, the high energy laser pulse can desorb intact molecules from the surface, and that some of the molecules are ionized and can be analyzed by mass spectrometry. The first application of laser desorption ionization was published in 1963 (Honing et al., 1963). Honing et al. irradiated various solids, conductors, semiconductors, and insulators in a vacuum with a focused beam from a pulsed ruby laser. Intense pulses of electrons and positive ions were produced as a result of the laser irradiation. In the late 1960's, Vastola et al. used a 100 mJ ruby laser with a 500 ns pulse to desorb organic salts and were able to obtain mass spectra up to 200 - 300 Da (Vastola et al., 1968 & 1970).

In 1978, Posthumus and coworkers presented laser desorption mass spectra of small biomolecules such as oligosaccharides, glycosides, amino acids, peptides, steroids, antibodies, and chlorophyll (Posthumus et al., 1978). These researchers used a pulsed laser with a two orders of magnitude lower power density than used Vastola et al. (Vastola et al., 1968 & 1970). However, until 1985, the upper mass range in laser desorption experiments

remained at about 2,000 Da (Lindner et al., 1985). A breakthrough result was obtained by Tanaka et al. in 1988. In Tanaka's experiments, the maximum molecular weight was extended to over 30,000 Da (Tanaka et al., 1988). At about the same time, Hillenkamp developed a method that they named "Matrix-Assisted Laser Desorption Ionization Mass Spectrometry (MALDI/MS)". With this method, spectra of compounds with molecular weights as high as 70,000 Da were demonstrated (Hillenkamp et al., 1988). A new era in biochemical mass spectrometry began with these discoveries. MALDI will be described in more detail in the following sections.

Matrix Assisted Laser Desorption Ionization (MALDI) Mass Spectrometry

History

In Tanaka's laser desorption ionization experiment, an extremely fine cobalt powder of about 300 Å diameter was suspended in a glycerol liquid and the suspension mixed with sample solution. A nitrogen laser (337 nm) was used for desorption ionization. Spectra were obtained of several proteins including carboxypeptidase A with a molecular weight of 34,000 Da. However, the mass resolution was low, about 20, and the signal to noise ratio was poor. Tanaka et al. suggested that the desorption mechanism in their experiments involved a laser induced heating of the extremely small metal particles, followed by heat conduction to the surrounding glycerol solution and a thermal desorption process. Tanaka's method was, however, largely forgotten.

Hillenkamp and coworkers developed an LD method that they named "Matrix Assisted Laser Desorption Ionization (MALDI)." These researchers mixed an absorbing material called a matrix, with the analytes. In their initial study, they used nicotinic acid as the matrix. A quadrupled Nd-YAG laser (266 nm) was used for desorption ionization. Spectra of proteins such as bovine albumin, trypsin, β -lactoglobulin, and lysozyme were obtained by this method. Nicotinic acid has a very strong absorption at 266 nm. It seems that the nicotinic acid absorbs the UV laser energy and provides the energy to the intermolecular degrees of freedom in the crystal. Since 1988, many MALDI matrices have been found. The selection of matrix can strongly affect MALDI spectra.

Advantages of MALDI

MALDI has many important advantages. The sensitivity is very high. Only femtomoles of analytes are typically required for MALDI analysis in favorable case (Karas et al.; 1989b). Furthermore, the maximum mass range in MALDI is around 500,000 Da although mass resolution decreases at high mass (Overberg et al., 1990). With a careful selection of the matrix compound, MALDI can be used for a very wide variety of biomolecules. Because of ease of use and high sensitivity, MALDI has become a dominant technique for molecular weight determination and structural characterization of large biomolecules.

Matrices in MALDI

Matrices in MALDI play a very important role, and their selection critically affect the MALDI spectra. There are two major requirements for good matrices in MALDI. First, the matrix must solvate and isolate the biomolecules in the crystal. Second, the matrix must

absorb the laser pulse with a high absorptivity (500 to $15,000 \text{ Lmol}^{-1}\text{cm}^{-1}$) at the given laser wavelength (Levis et al., 1994). Good MALDI results depend on the selection of matrix, the tolerance toward impurities, and the optimum molar ratio of matrix to analyte, usually $100:1$ to $50,000:1$ (Hillenkamp et al., 1991). Experience has shown that different matrices have different sensitivities toward impurities such as buffer salts and detergents. Choosing the best matrix to match analyte solution requirements is a determinant factor for obtaining good MALDI results. Also, the optimum ratio of matrix to analyte depends on the matrix used and on the size of the analyte molecules. Usually, the larger the analyte molecules, the larger the ratio of matrix to analyte should be.

Generally speaking, there are three functions that the matrix needs to serve in MALDI (Karas et al., 1989). First, an excess of matrix prevents aggregation of the large biomolecules and reduces the intermolecular forces. Furthermore, the matrix has to co-crystallize with the analytes. Beavis et al. demonstrated that proteins that were not incorporated into the matrix lattice also were not detected in the gas phase (Beavis et al., 1993). Second, the matrix absorbs the laser energy via electronic excitations, transfers the energy into vibration of the solid lattice and induces the necessary strong perturbation and disintegration of a microvolume. Third, the matrix must give a high ionization yield of analytes by photochemical reactions, most probably via radical intermediates. In several studies, the ion to neutral yield for the MALDI laser-desorption process has been estimated to be $1:10^4$ to $1:10^5$ (Mowry et al., 1993; Ens et al., 1991; Spengler et al., 1991). In these studies, ionic and neutral products of MALDI were simultaneously detected in a reflectron time-of-flight mass spectrometer. The neutrals were photoionized with coherent vacuum

ultraviolet radiation. Based upon relative signal intensities of directly formed analyte ions and photoionized analyte neutrals, the ratio of neutrals to ions was obtained (Mowry et al., 1993).

Most matrices used in MALDI are acids that contain an aromatic ring and a carboxylic group. For example, nicotinic acid, benzoic acid derivatives, and cinnamic acid derivatives are common matrices for UV/MALDI. However, an aromatic ring with a carboxylic acid group is not strictly required. Fitzgerald and coworkers have reported several basic matrices such as benzene derivatives containing amino groups (Fitzgerald et al., 1993). With such matrices, also acid-sensitive compounds can be analyzed by MALDI. Table 1 shows a summary of common matrices used with either UV or IR lasers.

Table 1. Summary of common matrices in MALDI (Karas et al., 1987; Hillenkamp et al., 1991; Karas et al., 1991; Overberg, 1992)

Matrix	Form	Some usable wavelength
Nicotinic acid	solid	266 nm, 2.94 μ m, 10.6 μ m
2,5-Dihydroxybenzoic acid	solid	266 nm, 337 nm, 355 nm, 2.79 μ m, 2.94 μ m, 10.6 μ m
Sinapinic acid	solid	266 nm, 337 nm, 355 nm, 2.79 μ m, 2.94 μ m, 10.6 μ m
Succinic acid	solid	2.94 μ m, 10.6 μ m
Urea	solid	2.79 μ m, 2.94 μ m, 10.6 μ m
Thiourea	solid	266 nm, 2.79 μ m, 2.94 μ m, 10.6 μ m
Tris buffer (pH 7.3)	solid	2.79 μ m, 2.94 μ m, 10.6 μ m
Caffeic acid	solid	337 nm, 355 nm
Ferric acid	solid	337 nm, 355 nm
Vanillic acid	solid	266 nm
Ice (frozen aqueous solution)	solid	10.6 μ m
Glycerol	liquid	2.79 μ m, 2.94 μ m, 10.6 μ m
3-Nitrobenzyl alcohol	liquid	337 nm, 266 nm
2-Nitrophenyl octyl ether	liquid	266 nm
Triethanolamine	liquid	2.79 μ m, 2.94 μ m

Development of Liquid Matrices for Laser Desorption

As described above, Tanaka early used liquid glycerol with an extremely fine cobalt powder for laser desorption (Tanaka et al., 1988). However, the mass resolution was very poor. Partly for this reason, no other groups reported following up on Tanaka's work. MALDI almost exclusively uses solid matrices. Still, some groups have tried to find practical liquid matrices for MALDI because liquid matrices are expected to have important advantages. The advantages include: (1) allowing a method for continuous desorption from the same spot with excellent pulse-to-pulse stability (Lusting et al., 1991) (2) allowing for the analysis of a homogeneous solution of analyte(s) and preventing "sweet spots" (3) allowing for a direct interface with liquid separation system (Li et al., 1993).

Some UV-absorption liquids such as 3-nitrobenzyl alcohol (3-NBA) have been tried as matrices for UV-MALDI. However, problems with this matrix seem to be low mass resolution and high matrix background (Chan et al., 1994; Li et al., 1993; Yau et al., 1993). A second approach has been to dissolve a strong absorbing dye such as Rhodamine 6G in a non-UV absorbing liquid (Cornet et al., 1993). The mass resolution was again quite low, about 50. A third approach has been to use a fibrous material as a solid substrate to which a non-UV absorbing liquid was added. This method has been used to obtain high quality laser desorption mass spectra of porphyrins (Kim et al., 1994). A fourth approach has been to use IR-MALDI. Liquids like glycerol, triethanolamine, and water have absorption bands in IR range. Hillenkamp et al., have demonstrated a spectrum of lysozyme at 14,300 Da by using glycerol as the matrix in IR-MALDI (Overberg et al., 1990). They used a Q-switched Er-YAG laser which has a wavelength of 2.94 μm and a pulse duration of 200 ns.

Mechanisms of MALDI

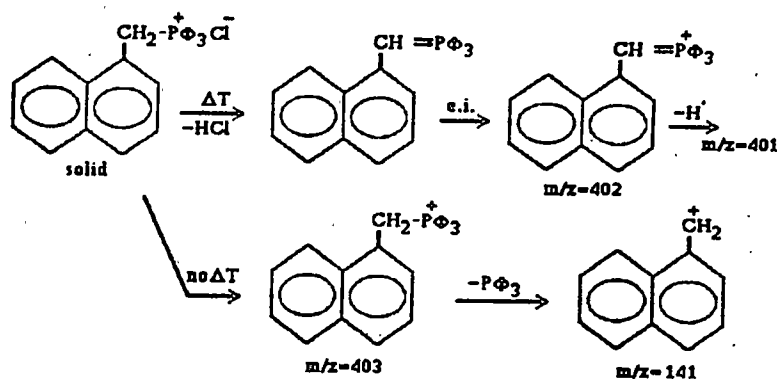
Since MALDI was introduced, many models and mechanisms have been proposed. To explain the MALDI process successfully, one question in particular must be answered. This is how the laser-induced process can transfer large molecules from the condensed phase to the gas phase without damaging the molecules (Vertes, 1991). The fundamental mechanisms of the MALDI process are still under active investigation. Some significant models will be described in the following.

Phase Explosion Model. Sunner et al. proposed a model called "phase explosion" for explaining the phenomenon of desorption ionization in liquid secondary ion mass spectrometry or FAB (Sunner et al., 1988b). This model can be equally well applied to the process in laser desorption since a high energy density is deposited in the material also in laser desorption.

The phase explosion model describes how the condensed phase transforms to a gas phase if the condensed phase is superheated, extremely rapidly to a high temperature. Above the temperature of "critical superheat", the matrix becomes mechanically unstable and undergoes a spontaneous "spinodal" decomposition. This phenomenon is called phase explosion or spinodal decomposition (Sunner et al., 1988b). The temperature for the "phase explosion" is $0.9 \times T_c$, where T_c is the critical temperature. It is explained that large molecules may survive intact despite the high energy density because of rapid cooling to a low temperature as the material transforms from the condensed phase to the gas phase. Furthermore, this model has been supported by a molecular dynamic simulation (Sunner et al., 1993). The

simulations showed that the spinodal decomposition mechanism can explain particle and laser desorption experiments

Cool Plume Model. This model was proposed by Vertes et al. (Vertes et al. 1988 & 1990a). It addressed the laser-solid interaction by describing the hydrodynamics of the laser-generated plume expansion. Subsequently, Balazes et al. refined this model (Balazes et al., 1991) to include also the phase transition, surface recession, and heat conduction processes in the solid, as well as electron-neutral inverse bremsstrahlung laser absorption, multiple ionization, and radiation cooling in the plume. The generated plume undergoes gas dynamic expansion and exhibits cooling. Two distinct time domains can be recognized in this model. The first time domain covers the time when the solid phase has not yet reached the phase transition temperature. This means that there is only a hot spot on the surface of the solid phase. The second time domain starts when the solid phase has been heated to the phase transition temperature. A dense plume is formed, and reactions like protonation, cationization, and adduct ion formation are proceeding in this plume. Subsequently, the temperature of the plume drops to a very low value due to expansion cooling. This cooling has a stabilizing effect on the entrained large molecules. An experiment using the fragmentation of a thermolabile compound, aryltriphenylphosphonium halide as a "thermometer" was claimed to support this model (Claereboudt et al., 1991). The fragmentation pathway is shown below (Claereboudt et al., 1991).



Ionization pathways of 1-naphthylmethyl-triphenylphosphonium chloride through thermal decomposition (ΔT) and in the absence of thermal decomposition (no ΔT).

This pathway has been studied and confirmed separately by electron impact, fast atom bombardment and laser desorption mass spectrometry. Without nicotinic acid present, thermal decomposition product ions, such as the ions at $m/z=401$ and 402 , appeared in the mass spectrum. With nicotinic acid matrix added, product ions, such as the ion at $m/z=403$, obtained from low internal energy aryltriphenylphosphonium ions were observed. No ions at $m/z=401$, 402 were found in the mass spectrum with nicotinic acid added. This showed the MALDI process including a strong cooling mechanism since none of laser-induced decomposition ions were formed.

Homogeneous Bottleneck Model. How can thermally labile molecules survive the very high energy density deposition used in MALDI? According to the homogeneous bottleneck model, there are two possibilities. Large molecules may survive due to an inefficient energy transfer process between matrix and analyte molecules (Vertes et al., 1990c). An additional cooling may result from two processes, phase transitions and heat conduction. Two effective phase transition processes are evaporation and sublimation. Cooling by heat conduction is

important only on a time scale much longer than the laser pulse. According to the authors, poor energy transfer between matrix and analyte molecules results from the mismatch of matrix-analyte interaction frequencies and matrix vibrational frequencies. If the frequencies are mismatched, energy will not be efficiently transferred to analyte molecules. A kinetic model of the energy transfer processes showed that, at an appropriately high sublimation rate, the analyte molecules will be desorbed internally cold (Vertes, 1990). The faster the energy transfer into the lattice, the faster is the cooling by sublimation. According to the computations by Vertes et al., by decreasing the energy transfer rate from the matrix to the analyte, the fragmentation of analyte ions can be decreased. This implies that in order to minimize fragmentation one should (1) keep the amount of analyte molecules as low as practically possible (energy transfer vs. detectability), (2) use a matrix host molecule with as poor a frequency overlap with the frequencies of the biomolecules as possible, (3) use a host matrix with a low sublimation temperature, and (4) use a laser pulse short enough to promote volatilization as opposed to degradation.

Shock Wave Model. Lindner and Seydel proposed a "shock wave model" for the laser desorption ionization process (Lindner & Seydel, 1985). The authors compared LD mass spectra obtained from a thick layer of sample (20 μm) under high intensity laser irradiation (10^{11} W/cm^2) with spectra obtained from a thin layer of sample (1 μm) under low intensity laser irradiation (10^8 W/cm^2). They concluded that under high intensity laser irradiation, little fragmentation and a high molecular ion yield resulted from a laser-driven shock wave. However, under low intensity irradiation conditions, extensive fragmentation and low

molecular ion yield resulted from thermal decomposition. That means that under high intensity irradiation, the heating rate is very high such that the matrix can reach the phase explosion limit without damage to the analyte molecules. Vertes et al. proposed another shock wave-induced mechanism for laser desorption of large molecules in MALDI (Vertes et al., 1988 & 1989). A one-component, one-dimensional hydrodynamics model was developed to describe the expansion of laser-generated plumes in the ion source. The model revealed two hydrodynamic phenomena: first, a compression wave propagating toward the interior of the target that is responsible for the splashing of molten material from a crater, and second, a shock wave in the plasma plume leaving the target that causes the appearance of energetic ions (Vertes et al., 1989).

Photoionization model. Ehring et al. have proposed a photoionization model to explain ionization in LD (Ehring et al., 1992). The authors stated that photoionization is the initial ionization step and that this is followed by ion-molecule reactions to give the final product ions. The gas-phase ionization energy for common organic compounds is about 7.5-9 eV. The laser photon energy in the UV range is about half of this ionization energy. (The photon energy at is 4.6 eV at 266 nm, and it is 3.7 eV at 337 nm.). In order for the molecules to become ionized, multiple photon absorption is required. This may occur through a two-step resonance absorption mechanism.

Instrumentation for Laser Desorption (LD) Time of Flight (TOF) Mass Spectrometry

Three components of the LD instrumentation will be described: (1) laser ion source, (2) time-of-flight mass spectrometer, (3) ion detectors, and (4) signal processing equipment. The instrumentation for MALDI and SALDI is the same as for LD.

Laser Ion Source

Laser interaction with solids can result in an ultrafast heating rate of the material to a high temperature. Rapid heating which can be produced by pulsed lasers (10^8 - 10^{12} K/s (Levis, 1994)) allows for thermally labile compounds to desorb intact from a condensed phase. The lasers used to deposit energy vary widely in terms of pulse length (CW to fs), irradiance (50 kW/cm² to 100 MW/cm²), and wavelength (151 nm to 10.6 μ m). The most commonly used lasers in LD are ultraviolet (UV) and infrared (IR) lasers. Commercial instruments are typically equipped with a nitrogen UV laser for 337 nm.

Time-of-Flight Mass Spectrometer

The selection of a mass analyzer is critical to obtain the best result in laser desorption mass spectrometry. Since laser interaction with solids may produce completely unexpected ionic and neutral species, the detection of all masses from every laser shot with a high transmission analyzer is preferred. Several types of mass analyzers have been used. When laser desorption was combined with a magnetic sector mass analyzer, the sensitivity was not good due to the low duty cycle (Eloy et al., 1971). Time of flight (TOF) analyzer is a much better alternative for pulsed laser desorption because of high ion transmission, and because the time taken for

the time taken for all the ions to pass through the flight tube is close to the time between laser pulses. In the 1970's, LD/TOF still had problems with broad ion kinetic energy distributions and slow signal processing. However, many improvements have been made since then. The major limitations of the quadrupole and magnetic sector instruments with respect to detecting all masses, scanning speed, and low ion transmission are avoided by the TOF principle itself (Vertes et al., 1993). The basic principle of TOF will now be discussed.

Basic Principles. TOF/MS was first proposed by Stephens in 1946 (Stephens, 1946). The basic linear TOF/MS instrumentation is shown in Figure 1. It consists of an ion source, a flight tube, and a detector. The distance (s) between the ion source plate and the accelerating grid is of the order of 0.5 cm. A fixed voltage V is applied to the ion source plate whereas the grid is grounded. The electric field is $E = V/s$. Ions that originate at the ion source plate are accelerated in the ion source region. They will all have essentially the same kinetic energy in the drift region of the flight tube.

$$\text{Kinetic energy} = mv^2/2 = zeV \quad (1)$$

$$v = (2zeV/m)^{1/2} \quad (2)$$

where m = the mass of ion, v = velocity of the ion, e = the charge of an electron, and z = number of ion charges. Ions of different m/z have different velocities in the vacuum flight tube. The ions travel a flight tube distance, l , to the detector, and the time-of-flight is given by:

$$t = l/v = l(m/2zeV)^{1/2} \quad (3)$$

Flight tube distances (l) ranging from 15 cm to 8 meters have been utilized. Typical

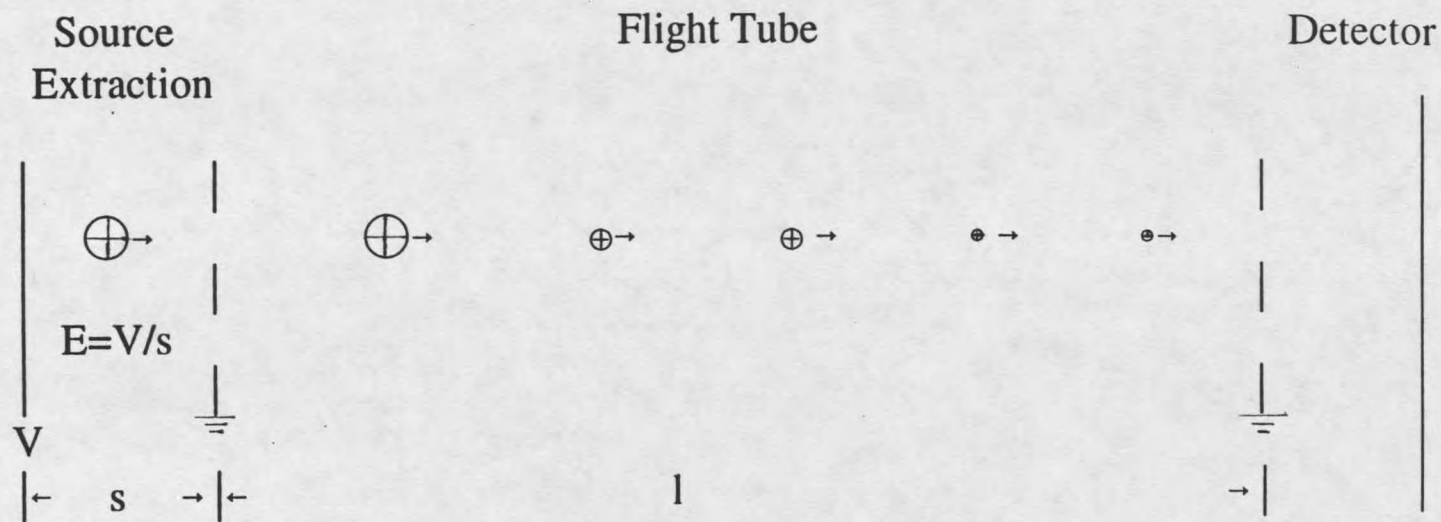


Figure 1. Linear time-of-flight mass spectrometer (from Cotter, 1994).

accelerating voltages (V) range from 3 kV to 30 kV, and typical flight times range from 5 to 100 microsecond (Cotter, 1994).

Advantages of TOF/MS. TOF/MS possesses many critical advantages (Price et al., 1994):

- (1) Ideal where ionization is pulsed.
- (2) Complete mass spectrum is obtained for each ionization event.
- (3) High ion transmission.
- (4) Fastest scanning mass spectrometer with repetition rates of up to 100 kHz.
- (5) High mass range (limited primarily by the detector).
- (6) Low cost.

Because TOF/MS has a very simple design and many advantages as described above, it has become the most popular mass analyzer for laser desorption.

Factors Affecting Mass Resolution of TOF. The mass resolution obtained in linear TOF/MS is usually fairly low. This is due to the time, space and kinetic energy distributions of ions as they fly from the ion source and through the flight tube (Cotter et al., 1992). Here, (1) the temporal distribution, (2) the spatial distribution, and (3) the kinetic energy distribution will be discussed.

(1) Temporal Distribution

Two ions with the same mass may be formed at different times during the ionization event but may still obtain the same kinetic energy in the flight tube. These ions will have different arrival times at the detector. This is referred to as the temporal distribution of the ions.

Because the mass resolution is determined by:

$$m/\Delta m = t/2\Delta t \quad (4)$$

when the time width of the arrival distance (Δt) is getting smaller, the mass resolution will be improved.

(2) Kinetic Energy Distribution

Another factor influencing the mass resolution in TOF/MS is the initial kinetic energy distribution. Ions of the same mass formed with different initial kinetic energies will have different arrival times at the detector, due to different velocities of ions through the flight tube.

(3) Spatial Distribution.

The mass resolution in TOF/MS will also be influenced by a spatial distribution. Ions of the same mass may be formed at the same time and with the same initial kinetic energy, but at different locations in the extraction field. These ions will experience a different acceleration voltage and will have different kinetic energies in the flight tube. They will arrive the detector at different times. This is referred to as the spatial distribution of ions.

Methods for Improving Mass Resolution in TOF/MS. Mass resolution in TOF/MS is affected by the temporal, spatial, and initial kinetic energy distribution as described above. By minimizing, or correcting, for these three distributions, mass resolution can be improved. Ionization by ultrashort pulsed lasers can minimize the uncertainties in the time of ion formation. The effects of the initial kinetic energy distribution can be minimized by using high extraction voltages or compensated for by a reflectron located in the mass analyzer

et al., 1994). The effects of the spatial distribution can be minimized by using low extraction voltages. Three techniques that have been used to improve the mass resolution in TOF/MS will be described: (1) two stage extraction (McLarne et al., 1955) (2) time lag focusing or delayed extraction (McLarne et al., 1955; Martin et al., 1995 & 1996), and (3) reflectron TOF/MS (Mamyryn et al., 1973).

(1) Two Stage Extraction

Because initial kinetic energy focusing demands a use of a high extraction voltages, one approach has been to use two-stage extraction. Two parallel grids define a low field extraction region above the sample plate and high field extraction region in front of the flight tube. For desorption techniques, in which ions are formed at a surface rather than in the gas phase, the spatial distribution is minimized. By accelerating ions in two source gaps with different electric fields, the mass resolution is improved (McLaren et al., 1955). However, the mass resolution still cannot be improved to more than about 1,000 Da with two stage extraction because the initial kinetic energy distribution cannot be compensated for by this method.

(2) Reflectron TOF/MS

Reflectron TOF/MS can solve the initial kinetic energy distribution problem. The principle was first proposed by Mamyryn in his Ph.D dissertation in 1966 (Mamyryn, 1966). The reflectron utilizes an electric field located at the end of the flight tube to reflect the ion trajectory around 180°, which is back along the initial flight path of the ions. A higher kinetic energy ion will penetrate the retarding field of the reflectron to a greater depth. Thus, high kinetic energy ions travel a longer distance, arriving at the detector at the same time as less

